Three-dimensional structure/function analysis of SCP-2-like2 reveals differences among SCP-2 family members[S]

David H. Dyer,*,† Vilena Wessely,† Katrina T. Forest,* and Que Lan[1,†]

Departments of Bacteriology* and Entomology,† University of Wisconsin-Madison, Madison, WI 53706

Abstract **Mosquito sterol carrier protein-2 (AeSCP-2) and sterol carrier protein-2-like2 (AeSCP-2L2) are members of the SCP-2 protein family with similar expression profiles in the mosquito life cycle. In an effort to understand how lipids can be transported by different SCP-2 proteins, the three-dimensional crystal structure of AeSCP-2L2 was solved at 1.7 Å resolution. AeSCP-2L2 forms a dimer and binds three fatty acids, one of which resides in a position within the internal cavity at a right angle to the others. This first report of ligand-bound dimerized protein in the SCP-2 protein family indicates that the family has a much more divergent mode of interaction with ligands than previously reported. The potential function of AeSCP-2L2 was investigated via in vivo incorporation of [^{3}H]cholesterol and [^{3}H]palmitic acid. Overexpression of *AeSCP-2L2* in mosquito cells leads to an increased uptake of free fatty acid, whereas knockdown of *AeSCP-2L2* in adult females decreases the accumulation of free fatty acid in the fat body from a blood meal. In contrast, overexpression or knockdown of *AeSCP-2L2* has no effect on cholesterol uptake. Our results suggest that the main function of AeSCP-2L2 is as a general intracellular fatty acid carrier, as opposed to having a dedicated role in cholesterol transport.**—Dyer, D. H., V. Wessely, K. T. Forest, and Q. Lan. **Three-dimensional structure/function analysis of SCP-2-like2 reveals differences among SCP-2 family members.** ***J. Lipid Res.*** **2008.** 49: **644–653.**

Supplementary key words mosquito • cholesterol • fatty acid • sterol carrier protein-2

The sterol carrier protein-2 (SCP-2) family includes proteins containing a sterol carrier domain (SCP-2 domain). The founding member of this family, SCP-2 itself, is a low molecular mass (12–15 kDa) single-domain protein. SCP-2 was first identified as an intracellular nonspecific lipid carrier (1). The vertebrate SCP-2 has been shown to facilitate lipid transfer between membranous vesicles in in vitro assays (2–4). SCP-2 also enhances lipid uptake and redistribution in cultured cells (5–10). However, the biological function of SCP-2 is subject to debate as a result of its ability to bind diverse ligands (11–13). Knockdown of SCP-2 in mice results in the disruption of both cholesterol and fatty acid metabolism (14, 15), implying that the vertebrate SCP-2 may be involved in general lipid metabolism. In vertebrate genomes, SCP-2 is transcribed from a single-copy SCP-x/SCP-2 gene (16, 17). In insect genomes, especially in Diptera, the SCP-2 gene has gone through expansion that predicts several low molecular mass SCP-2-like proteins in *Drosophila melanogaster* (CG11151 and CG12269), *Anopheles gambiae* (ENSANGP00000020493, ENSANGP00000026507, and ENSANGP00000020470), and *Aedes aegypti* (AAO34708, AAEL012696-PA, AAEL012697-PA, and AAEL012704-PA). Whether the insect SCP-2 and SCP-2-like proteins have redundant function is unknown.

The expression of the yellow fever mosquito SCP-2 (AeSCP-2) and SCP-2-like genes (AeSCP-2-like1 and AeSCP-2-like2) is overlapped temporally and spatially in the larval stages, but only AeSCP-2 and AeSCP-2-like2 (AeSCP-2L2) genes are transcribed in adults (18, 19). The ligand binding affinities of AeSCP-2 and AeSCP-2L2 are different: AeSCP-2 has substantially higher affinity (5.6×10^{-9} M) for cholesterol (20) than AeSCP-2L2 (2.6×10^{-6} M) (19). On the other hand, AeSCP-2L2's affinities for lipids are greater for fatty acids than for cholesterol (19). To further our understanding of the function of SCP-2L2, we solved its three-dimensional structure by X-ray crystallography and analyzed the effects of overexpression and underexpression of AeSCP-2 and AeSCP-2L2 on lipid uptake in vivo.

MATERIALS AND METHODS

Chemicals

Chemicals and reagent were purchased from Sigma (St. Louis, MO), Fisher Scientific (Pittsburgh, PA), and ICN (Costa

Manuscript received 11 October 2007 and in revised form 26 November 2007 and in re-revised form 14 December 2007.

Published, JLR Papers in Press, December 15, 2007.
DOI 10.1194/jlr.M700460-JLR200

[1] To whom correspondence should be addressed.
e-mail: qlan@entomology.wisc.edu

[S] The online version of this article (available at http://www.jlr.org) contains supplementary data in the form of one table and one figure.

Mesa, CA) if their origins are not mentioned in the text. [1,2-^{3}H(N)]cholesterol (40 Ci/mmol) and [9,10-^{3}H]palmitic acid (60 Ci/mmol) were purchased from American Radiolabeled Chemicals, Inc. (St. Louis, MO). All DNA primers were synthesized by IDT (Coralville, IA) unless noted otherwise.

Purification of recombinant AeSCP-2L2

AeSCP-2L2 was cloned into a pGEX-4T-2 glutathione *S*-transferase (GST) affinity tag vector (Amersham Biosciences, Piscataway, NJ) as described (19). The resulting plasmid, pSCP2L2-GST, was transformed under ampicillin selection into *Escherichia coli* strain BL21. The purification methods used are identical to those that yielded protein for the AeSCP-2 crystal structure and have been described previously (21). Briefly, after thrombin cleavage to release AeSCP-2L2, thrombin was removed on a benzamidine column (Amersham Biosciences) equilibrated with phosphate-buffered saline. Purified protein was concentrated in Ultracel-10K centrifugal filters (Millipore, Billerica, MA) with a 10,000 molecular weight cutoff. When the volume reached ~10 ml, the protein was transferred to a Centricon YM-3 (Amicon, Beverly, MA) for further concentration to 15–20 mg/ml. Protein concentration was measured using a Nanodrop spectrophotometer (NanoDrop Technologies, Wilmington, DE) and the calculated extinction coefficient. The protein was placed in a Slide-A-Lyzer dialysis cassette (Pierce, Rockford, IL) and dialyzed against 4 liters of 25 mM KCl and 50 mM HEPES (pH 7.5) for 20 h at 4°C. The molecular weight of recombinant AeSCP-2L2 was verified via mass spectroscopy (19). The final protein concentration was adjusted to 10 mg/ml with dialysis buffer, and the protein was drop-frozen in liquid nitrogen and stored at −80°C.

Crystallization and data collection

Crystals of AeSCP-2L2 were grown at room temperature using the hanging drop technique and were first identified from a commercial sparse matrix screen (Qiagen, Valencia, CA). The AeSCP-2L2 native data were collected to 1.7 Å at −180°C. The space group was identified as $P2_1$, with unit cell constants of a = 45.4 Å, b = 56.4 Å, c = 50.6 Å, and γ = 119.4°. To grow the crystals, 2 μl of AeSCP-2L2 at 10 mg/ml was combined with 2 μl of the well solution containing 1.6 M sodium citrate, 5% glycerol, and 100 mM HEPES, pH 7.5. Unusable large jagged block crystals formed after 3–4 days. Streak seeding of the shattered remnants of the initial crystals with a horse whisker into a more dilute mother liquor yielded useful cubic and tetrahedral crystals. The initial mother liquor diluted by adding 100 to 150 μl of water to the well solution before streak seeding to slow the nucleation. The addition of 400 mM NaCl to a synthetic mother liquor of 1.6 M sodium citrate, 10% glycerol, and 100 mM HEPES (pH 7.5) resulted in a significantly lower mosaic spread in the data when the native crystals were flash-cooled directly into liquid nitrogen.

Crystals used for multiple isomorphous replacement were treated for 2 weeks at room temperature with heavy atom compounds. Three successful isomorphous derivatives ($OsCl_3$, K_2PtCl_4, and K_2PtCl_6) were prepared by dissolving 10 mM heavy atoms solubilized in 1.5 M sodium citrate, 5% glycerol, 400 mM NaCl, and 100 mM HEPES, pH 7.5 (Hampton Research, Aliso Viejo, CA). These stock solutions were added directly to ~1 week old drops containing the AeSCP-2L2 crystals to achieve a final derivative concentration of 5 mM. Crystals were not back-soaked; rather, they were flash-cooled directly into liquid nitrogen. A room temperature native data set was also collected to 2.0 Å resolution by means of capillary mounting a relatively large AeSCP-2L2 crystal (0.5 × 0.4 × 0.4 mm). In the room temperature data set, the unit cell was slightly different, with unit cell constants of a = 46.3 Å, b = 57.3 Å, c = 49.1 Å, and γ =114.5°.

Data collection was done in-house on a Proteum CCD detector (Bruker AXS). Data were processed and scaled using Proteum 2 software (Bruker AXS). Heavy atom binding sites were identified, and the positions, B-factors, and occupancies were refined with Sharp (22). The overall figure of merit for the initial phased map was 0.387/0.467 (centric/acentric). The initial phases allowed ARP/warp (23) to trace 35 residues in a total of five alanine chains. The model was improved using iterative cycles of refinement in Refmac5 (24) and manual building with Xfit (25) to produce the finished structure. All native amino acids of both chains are accounted for, and residues Gly^{-3}, Ile^{-2}, and Arg^{-1} in chain A and Ser^{-4}, Gly^{-3}, Ile^{-2}, and Arg^{-1} in chain B (expression tag residues remaining after thrombin cleavage of the recombinant protein) are also resolved. The final R-factor for the cryo temperature structure is 19.7% (R-free with 5% of data omitted 23.5%). For the room temperature structure, R and R-free are 18.8% and 22.9%, respectively. Omit maps reduced model bias and clearly showed the positions of the three fatty acids. Structure and coordinate analysis with Procheck (26) revealed that 94.1% (93.5% in the room temperature data set) of the nonglycine, nonproline amino acids lie within the most favored regions of the Ramachandren plot, with all remaining residues in the additionally allowed region.

Mosquitoes

The mosquitoes used in these experiments, *Aedes aegypti*, were taken from an inbred laboratory strain (Rockefeller). Larvae were reared at 26°C in 70–80% humidity with a light/dark cycle of 14 h/10 h with fish food (TretraMin; Tetra Holding, Inc., Blacksburg, VA). Larvae hatching during a 15 min period were collected and used in the experiments. Under these conditions, the development takes 64 h (mostly males) to 72 h (mostly females) to complete the fourth stadium. Adults were maintained at 26°C. Female adults were given defibrinated rabbit blood meals (Lampire Biological Labs, Inc., Pipersville, PA) via a glass feeder (Lillie Glassblowers, Atlanta, GA) covered by a thin layer of membrane; the glass feeder was kept at 37°C through the circulation of water heated to 37°C. Blood-fed females lay eggs between 74 and 76 h after the blood meal.

Cell cultures and lipid incorporation in Aag-2 cells

The *A. aegypti* cell line Aag-2 was maintained in Eagle's medium (Invitrogen Corp., Carlsbad, CA) supplemented with 5% fetal bovine serum (27) at 28°C under a 5% CO_2 atmosphere. Passages of cells were conducted every 7 days with a 1:5 dilution of cells.

AeSCP-2L2 overexpression vector was constructed by inserting the entire coding sequence of *AeSCP-2* into the pIE1^{hr} expression vector (28). The coding sequence of the Enhanced Green Fluorescent Protein (EGFP) gene from the pEGFP vector (Clontech, Mountain View, CA) was cloned into the pIE1^{hr} expression vector, and the EGFP overexpression vector was used as a transfection control. The overexpression vectors were sequenced to ensure that the insertions were in the correct orientation and that the coding sequences were unaltered. High-quality plasmid DNA was purified using Maxprep columns (Qiagen). DNA concentration was determined by the ultraviolet (UV) light absorbance at 260 nm.

Aag-2 cells were seeded at 0.5 ml of 5×10^5 cells/ml in 24-well culture dishes. After overnight incubation, culture medium was removed and the cells were washed once with 0.5 ml of transfection medium (without serum and antibiotics). One-half milliliter of transfection medium containing 4 μg/ml AeSCP-2L2

overexpression vector and 8 μg/ml lipofectin (Invitrogen) was added into each well of cell cultures. Control transfected cells were treated with transfection medium containing 4 μg/ml EGFP overexpression vector and 8 μg/ml lipofectin. Cells were incubated in transfection medium for 8 h, and the transfection medium was replaced with 2 ml of fresh medium and incubated at 28°C.

Culture medium was removed at 36 h after transfection, and 0.5 ml of fresh steroid-free medium was added (27). After overnight culture in steroid-free medium, the medium was replaced with 0.5 ml of steroid-free medium containing 0.33 μCi [^{3}H]cholesterol/ml or 3.3 μCi [^{3}H]palmitic acid/ml and incubated for 12 h. Cells were washed twice with 1 ml of cold PBS, and the total cellular lipids were extracted as described (5). Cellular [^{3}H]cholesterol was quantified in a liquid scintillation counter (Packard, Billerica, MA). The content of cellular [^{3}H]cholesterol or [^{3}H]palmitic acid is given as dpm/mg total protein. The levels of lipid incorporation were normalized to the control (EGFP overexpression), which was arbitrarily set at 1. The tests were performed two times in triplicate each time (for a total of six data points).

DsRNA-mediated RNAi

Two 21 bp complementary primers for AeSCP-2L2 gene silencing were designed. The primers matched to the N-terminal portion of the AeSCP-2L2 sequence were targeted. An 8 base T7 primer sequence was added to the sense and the antisense targeted sequences 5′-**aatgattctctcgatgatagt**cctgtctc-3′ and 5′-**aaactatcatcgagagaatca**cctgtctc-3′ (boldface letters represent coding sequences) for in vitro transcription. High-quality dsRNA was produced using an RNAi construction kit (Silencer™; Ambion, Austin, TX). Chemically synthesized AeSCP-2 dsRNA (Ambion) used primers 5′-**uagcgaucuuggcgaaaac**tt-3′ and 5′-**guuuucgccaagaucgcua**tt-3′ (boldface letters represent coding sequences). Two 21 bp complementary primers were chosen from the green fluorescent protein (GFP) coding region to be used as the RNA interference control: the sense (5′-**cucccacaacguauacauc**tt-3′) and antisense (5′-**gauguauacguuucuggag**tt-3′) (boldface letters represent coding sequences) dsRNA primers were synthesized by Ambion. The quantity of GFP dsRNA was determined by UV at 260 nm.

Day 1 females were anesthetized at 4°C, and 0.5 μl of dsRNA (35–70 μmol) was injected intrathoracially as described (29). GFP dsRNA was used as a microinjection control. Microinjected females were put back into a cage containing males and maintained at 26°C in 70–80% humidity with access to 10% glucose until a blood meal was given.

RNA extraction and RT-PCR

Three females from dsRNA treatments were randomly selected from each treatment to determine the effect of dsRNA-mediated gene expression knockdown. Females were anesthetized at 4°C, and each chosen female mosquito was put into a 1.5 ml Eppendorf test tube and homogenized with a micropestle in 1 ml of Trizol reagent according to the manufacturer's instructions (Invitrogen). The quantity of total RNA was determined by UV light absorption at 260 nm. The RNA samples were frozen at −80°C until use. Total RNA from each sample was treated two times with RNase-free DNaseI according to the manufacturer's description (DNA-free™ kit; Ambion). The cleaned RNA samples (0.4 μg) were subjected to 35 PCR cycles with *AeSCP-2* or *AeSCP-2L2* gene-specific primers to ensure that there was no genomic DNA contaminant in the RNA samples (data not shown). Transcripts of *AeSCP-2L2* were determined in the dsRNA-treated samples using a pair of gene-specific primers (5′-atgtctgtggaaactatcatcgag-3′ and 5′-ttaaatcacttcagccagcttagc-3′). Internal control for the RT-PCR is the *A. aegypti Act-2* (30) using gene-specific primers in the 3′ untranslated region: 5-cgaactcctccagccactac-3′ and 5′-gcagtttcctagcggttgtc-3′. The RT-PCR was carried out in a 12.5 μl volume with 0.4 μg of total RNA using Phusion High-fidelity PCR Master Mix (New England Biolabs, Ipswich, MA). RT-PCR conditions were as follows: an initial 98°C cycle for 30 s, followed by 27 cycles of 98°C for 10 s, 60°C for 30s, and 72°C for 15 s.

Cholesterol and fatty acid incorporation in vivo

Seventy-two hours after microinjection of dsRNA, females were given an artificial blood meal (31) containing 1 μCi of [^{3}H]cholesterol or 10 μCi of [^{3}H]palmitic acid. Females that took a full blood meal were separated into a cage with access to 10% glucose and maintained at 26°C in 70–80% humidity. Seventy-two hours after the blood meal, ovaries and fat bodies were dissected from each female, and the cellular lipids were extracted as described (5) with minor modifications. Each tissue from each female was placed into a 1.5 ml Eppendorf tube and homogenized in 100 μl of isopropanol using a micropestle, another 100 μl of isopropanol was used to rinse the micropestle in the tube, and 300 μl of hexane was added into the tube (isopropanol-hexane = 2:3). The homogenate was vortexed at room temperature for 1 min and centrifuged at 2,000 *g* for 15 min at 4°C. The supernatant, the organic phase containing cellular lipids, was removed to a glass scintillation vial and air-dried. Radioactive cholesterol or palmitic acid in the lipid extract was measured in a scintillation counter (Packard). The protein pellet from each sample was air-dried and dissolved in 100 μl of buffer (1% SDS, 5 mM EDTA, and 250 mM Tris-HCl, pH 8.0) at 37°C overnight and centrifuged at 12,000 *g* at room temperature for 10 min, and supernatant (soluble cellular protein) was collected. Protein concentrations were determined using a BCA kit (Pierce, Rockford, IL). The content of cellular [^{3}H]cholesterol or [^{3}H]palmitic acid is described as dpm/mg total protein.

RESULTS

The three-dimensional structure of SCP-2L2

The protein structure of AeSCP-2L2 in complex with three fatty acids was determined at 1.7 Å resolution by multiple isomorphous replacement and anomalous dispersion (**Table 1**). It is the first example of a liganded homodimeric structure within the SCP-2 superfamily (**Fig. 1A**). The recombinant AeSCP-2L2 protein has a predicted molecular mass of 11,665 Da (19). Gel filtration analysis of purified recombinant AeSCP-2L2 yielded a molecular mass of ∼19 kDa (see supplementary Fig. I), indicating that purified recombinant AeSCP-2L2 is a homodimer in solution. Therefore, the homodimeric structure of AeSCP-2L2 is not an artificial phenomenon induced via the protein crystallization process. AeSCP-2L2 exhibits an α+β tertiary classification (Fig. 1A) with a five-stranded antiparallel β sheet in the order 3-2-1-4-5, as defined by structural classification of proteins (32). The four α helices occur prior to β1 (α1), between β4 and β5 (α2 and α3), and after β5 (α4). There are two monomers in each crystallographic asymmetric unit, related by a root mean square difference of 0.7 Å over all 216 Cα atoms. Interestingly,

TABLE 1. Data collection and refinement statistics

	Native	Native	$OsCl_3$	K_2PtCl_4	K_2PtCl_6
Protein Data Bank identifier	2QZT	3BDQ			
Data collection temperature (°C)	−180	+23	−180	−180	−180
Total reflections	84,952	73,210	40,292	26,480	40,592
Unique reflections	24,343	14,850	11,190	7,700	5,565
Resolution (Å)[a]	25.0–1.7 (1.7–1.76)	25.0–2.0 (2.0–2.05)	25.0–2.7 (2.7–2.8)	25.0–2.5 (2.5–2.55)	25.0–2.8 (2.8–2.9)
R-merge (%)[b]	0.083 (0.108)	0.045 (0.207)	0.031 (0.098)	0.059 (0.191)	0.036 (0.072)
Completeness (%)	98.1 (89.7)	93.7 (91.4)	98.1 (86.3)	97.3 (83.4)	98.8 (96.5)
Average I/Σ	16.2 (4.9)	21.2 (4.6)	26.9 (9.8)	14.1 (5.3)	21.9 (9.3)
Riso on F			0.097	0.147	0.236
Riso on I			0.161	0.241	0.433
Number of sites			2	3	2
Phasing power (centric/acentric)			0.205/0.212	1.34/1.47	0.662/0.712
Phasing power (anomalous)			0.073	0.294	0.537
Number of molecules per asymmetric unit	2				
Number of fatty acid ligands	3				
Number of solvent atoms	188	68			
R-factor (%)	19.7 (22.2)	18.8 (19.3)			
R-free (%)	23.5 (23.5)	22.9 (24.5)			
Mean B value ($Å^2$)	17.4	21.4			
B value vertical fat chain A	31.4	33.6			
B value horizontal fat chain A	33.2	37.6			
B value vertical fat chain B	32.1	36.2			
Estimated standard uncertainties (maximum likelihood)	0.076 Å	0.107 Å			
Root mean square deviation bond length	0.014 Å	0.010 Å			
Root mean square deviation bond angles	1.42°	1.14°			

[a] Values for the highest resolution shells are shown in parentheses.
[b] R-factor = $(\Sigma|Fo - Fc|/\Sigma|Fo|) \times 100$, where F_o is the observed structure-factor amplitude and F_c is the calculated structure-factor amplitude.

the tertiary structure of the AeSCP-2L2 fold is closely related to the previously determined structure of AeSCP-2 (23), with a root mean square difference of 1.5 Å over 88 amino acids, even though the identical residues shared between AeSCP-2 and AeSCP-2L2 number only 25 (28.4%), whereas the sequence homology is 81% (21). In addition to the dimeric nature of AeSCP-2L2, notable differences between the mosquito SCP-2 and SCP-2L2 X-ray structures include the mode of fatty acid coordination, the size and shape of the cavity, and the length of the C-terminal helix.

Unexpected dimer interface

The two protein chains within each crystallographic asymmetric unit form a novel homodimer with potential biological implications. The interface-accessible surface area buried per monomer is 663 $Å^2$, constituting 10.1% of the total surface area of SCP-2L2, as calculated with the protein-protein interaction server (V1.5) comparing the chain A interface with chain B (http://www.biochem.ucl.ac.uk/bsm/PP/server/). This total buried surface area compares favorably with 32 analyzed homodimeric proteins (33). The residues involved in the formation of the homodimer from both chains A and B include Gly81, Leu84, Lys85, Gly87, Leu91, Ser92, Gly93, Asp94, Ala95, Asp96, Ala99, Ala102, and Glu103 (Fig. 1B). The packing of chains A and B to form the symmetric homodimer includes 13 of the 25 C-terminal residues from each polypeptide; chain A α3 contacts chain B α3 and α4, whereas the β5-α4 loop packs across the noncrystallographic symmetry axis against the same element in the opposite monomer. The symmetrically related interface residues that position the 180° rotational flip of chains A and B in relation to one another involve Gly81 and Gly93 (Fig. 1B).

A large cavity accommodates unexpected horizontal ligand

A large branched internal cavity holds three C16 fatty acids (see supplementary Table I) by coordination through the carboxylate groups of the fat near outer openings to the surface of AeSCP-2L2. The fats were identified unequivocally as palmitic acids based on omit map electron density (**Fig. 2**). The tunnel is sandwiched between β sheets and α-helices and is calculated without fats or waters present to have a volume of 2,968 $Å^3$, as determined with Sybyl (www.tripos.com) using the Fast Connolly Channel method with a probe radius of 1.4 Å (34). The channel contains one horizontal lipid binding site that holds a fat that nearly transverses the dimer interface plus two vertical lipid binding sites each contained within each monomer.

The horizontal lipid of AeSCP-2L2 breaks the true 2-fold symmetry of the SCP-2L2 dimer and is the likely cause for the area of greatest discrepancy between the two monomer folds, as α2 and α3 are pushed toward the outer surface of the protein to accommodate the head group and long tail of palmitate, respectively (Fig. 1A). The hydrophobic tunnel passing through the center of the protein is oriented in a similar manner to that observed previously in the mammalian SCP-2 folds, which include an unliganded rabbit SCP-2 and the Triton X-bound SCP-2-like domain of the human multifunctional enzyme (Mfe) (**Fig. 3**) (35, 36). The outer opening of the hori-

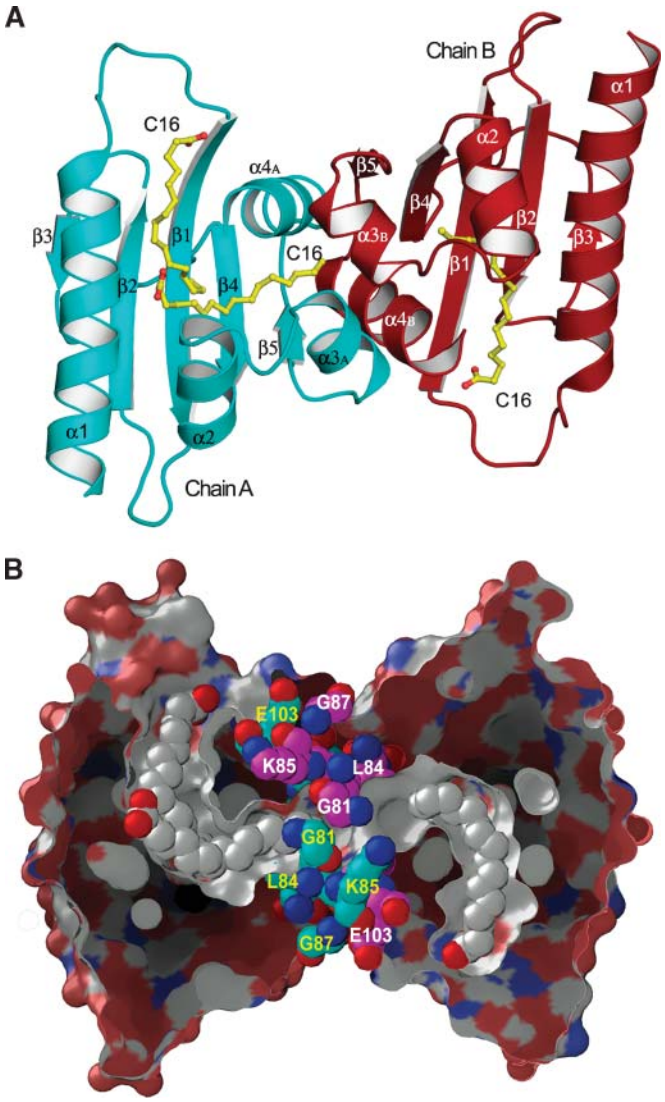

Fig. 1. The final refined structure of AeSCP-2L2 [Protein Data Bank No. (PDB) 2QZT] bound to C16 fatty acids. A: SCP-2L2 (chain A, cyan; chain B, red) binds three palmitate ligands (yellow). B: Surface representation cut through the middle to reveal a hydrophobic cavity with ligands. The residues at the homodimeric interface provide the surface area for dimerization. The selected space filled residues have carbon atoms colored to correspond to the polypeptide chain to which they belong (chain A, cyan; chain B, magenta). The structure is oriented in a similar position to A to emphasize the ~2-fold symmetry.

zontal cavity of chain A is composed of α1 residues Arg9 and Arg13, α2 residues Ile73, Ser74, and Lys76, and α4 C-terminal residue Ile105. Residues Arg13 NH_2 (2.6 Å) and Ser74 OG (2.7 Å) coordinate the carboxylate group on opposite sides of the oval opening to the horizontal cavity (Fig. 2). There are also two water molecules observed within H bonding distance nearly equidistant from the O1 and O2 of the palmitate. The orientation of these side chains positions the horizontal ligand through the interior of the cavity, threading it toward the dimer interface. The position of the last carbon of the acyl chain is 4.2 Å from Leu84 on chain B. Interestingly, there is no electron density in the corresponding location of the cavity entrance on chain B, even though the cavity is slightly larger than in chain A as a result of alternative conformations of residues Ile6 and Met70, which are modeled as having two different rotomers in the cavity of chain A. Superposition of chain A on chain B shows the horizontal cavity entrance environment on chain B to have two waters slightly buried. The presence of the two waters causes a positional displacement of Arg13 NE and Ser74 OG, effectively creating a slightly larger entrance to the internal tunnel relative to their counterparts on chain A that bind the horizontal ligand.

In the previously solved AeSCP-2 structure, Arg15 occupies a similar position to Arg13 in AeSCP-2L2, but rather than forming a direct salt bridge it coordinates a water molecule that is hydrogen bonded to the vertical C16 fat. Superposition of the insect structures of AeSCP-2 and AeSCP-2L2 shows the interior cavity of AeSCP-2 to be inadequate to coordinate a horizontal lipid without a rearrangement of the last four residues (ASLK) on the C-terminal helix of AeSCP-2. At the opposite side of the AeSCP-2 pocket, which could mimic the horizontal cavity of AeSCP-2L2, there would need to be a rearrangement of residues Val96, Phe100, and Ile101 in AeSCP-2 to accommodate another ligand.

Vertical cavities

The vertical cavities of AeSCP-2L2 that connect to each other through the horizontal cavity are composed of β sheet secondary structure and the N-terminal and C-terminal helices, which provide a hydrophobic environment for the acyl tails of the fatty acids (Fig. 1B). The vertical cavity of AeSCP-2L2 is directly comparable to the ligand cavity in the only other insect SCP2 structure solved to date, AeSCP-2 (21). The C16 fats bind in a similar orientation when AeSCP-2 is superimposed upon AeSCP-2L2, although the coordination of the vertical fat in AeSCP-2L2 is different, giving the appearance of kinking the carboxylate head group at the C2 of the acyl chain (Fig. 3). The differences in the orientation of the acyl tail are primarily attributable to the hydrophobic residues lining the cavity for each protein (all atomic distances for the residues within proximity of the three C16 fats are listed in supplementary Table I). In AeSCP-2L2, residues Leu31 and Val44 occupy similar positions in the hydrophobic cavity as residues Phe32 and Met46 in AeSCP-2, thereby causing the positional differences of the acyl chain. The fatty acid coordination in the vertical position of AeSCP-2L2 and AeSCP-2 is also quite different for the carboxylate moiety. In AeSCP-2L2, O2 of the fat carboxylate group is coordinated via hydrogen bonds to the amide backbone of residue Lys24 and to a water molecule (Fig. 2). O1 forms hydrogen bonds with the backbone amide of Val25, with an apparently penta-coordinated water molecule. The water itself forms hydrogen bonds with the NH_1 and NE of Arg23 along with the main chain oxygens of Val25 and Leu46. This hydrogen bonding net is in contrast to AeSCP-2, in which the C16 fatty acid moiety is coordinated with two water molecules along with the NH_1

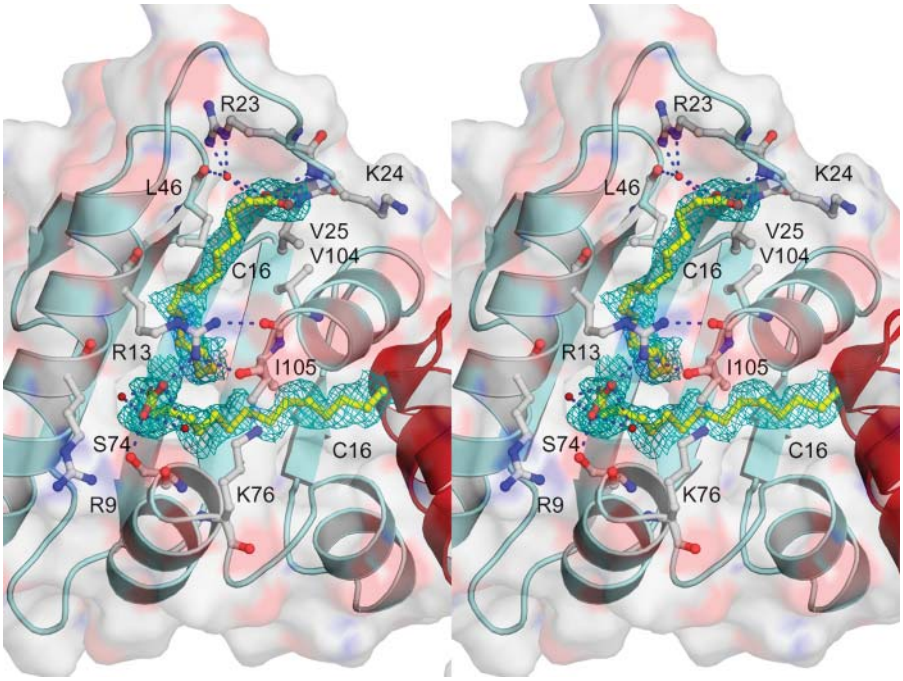

Fig. 2. Vertical and horizontal lipid binding sites. A stereo view closeup of chain A amino acid residues coordinating carboxyl moieties of both fats emphasized by the corresponding electron density from the Fo-Fc map calculated without ligand (cyan), contoured at 1σ. Fo is the observed structure-factor amplitude and Fc is the calculated structure-factor amplitude.

and NE of Arg24 and main chain oxygen of Gln25 (21). It is notable that even though coordination of the C16 fats in the vertical position in AeSCP-2L2 versus AeSCP-2 is so different, fats are oriented in a similar manner within the cavity. Evolution of the α1-β1 loop region may explain how diverse members of the SCP-2 family have retained the ability to bind and carry a wide variety of ligands, such as cholesterol, phospholipids, and lipids. As the mosquito SCP-2 is only known to bind palmitic acid in the vertical orientation (21), our discovery that AeSCP-2L2 possesses both vertical and horizontal ligand binding sites comes as a second novel result, in addition to the dimeric nature of the liganded AeSCP-2L2.

AeSCP-2L2 cryo and room temperature models

In addition to the 1.7 Å cryo-cooled data set of AeSCP-2L2, a room temperature data set was collected and the structure refined to 2.0 Å to identify differences between the cryo crystallographic model and one generated at room temperature (3BDQ). There is mounting evidence that there can be unforeseen consequences to the commonplace cryopreservation techniques compared with data collected at room temperature (35, 36). The most obvious difference between the models is attributable to contraction of the bulk solvent within the lattice during the vitrification process. The change in the unit cell volume of the cryo-cooled structure (112,878 $Å^3$) was ~5% smaller than in the room temperature structure (118,533 $Å^3$). There were 188 waters modeled in the flash-cooled structure, as opposed to only 68 waters identified in the room temperature data, consistent with the contraction of the unit cell. Of the 68 waters modeled in the room temperature structure, nearly all of them (>90%) have counterparts in the flash-cooled model. The most obvious differences can be seen in the vicinity of the cavity opening on chain B that corresponds to the position that is apo for the horizontal ligand. In the low-temperature model, this cavity opening shows the side chain of Lys76 to move toward the protein, thereby decreasing the width of the observed opening and trapping two water molecules below the surface slightly within the cavity. At the same position in the room temperature model, the terminal amino group of Lys76 swings away from the protein by 4.0 Å, which leaves a much wider cavity opening, and the waters observed in the flash-cooled model are not present.

Another aspect of having both low- and high-temperature AeSCP-2L2 structures is the ability to analyze the occupancy (B-factors) for the palmitic acid moieties at the different binding sights. Although the resolution of the data is different, 1.7 Å (low temperature) versus 2.0 Å (room temperature), there is a trend that is very comparable between the two models (Table 1). The vertical fat in chain A has the lowest B-value, followed by the vertical fat in chain B. The horizontal fat in chain A has the highest B-value in both models, yet the difference between the highest occupied fat (the vertical fat in chain A) is only 6.5% from the horizontal fat in chain A in the low-temperature model, compared with a difference of 9.5% in the room temperature model. Perhaps the effect of the constraints placed on the lattice by cryopreservation.

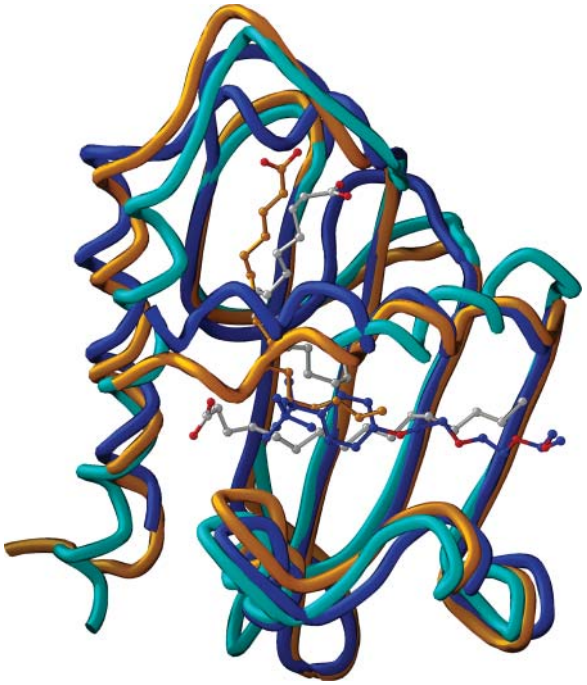

Fig. 3. Backbone comparison of known liganded SCP-2 family members. Superposition of the AeSCP-2L2 (PDB 2QZT; cyan) chain A with C16-bound AeSCP-2 (PDB 1PZ4; yellow brown) and the SCP2 domain of human multifunctional enzyme Mfe-2 (PDB 1KTA; dark blue) bound to Triton X-100.

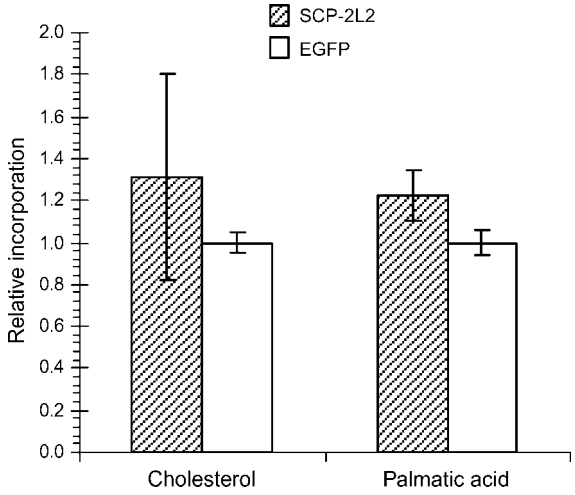

Fig. 4. Effect of *AeSCP-2* and *AeSCP-2L2* overexpression on lipid uptake in cultured mosquito cells. An Enhanced Green Fluorescent Protein (EGFP) expression vector was used as the transfection control. Incorporation of lipid is normalized to the level of EGFP overexpression in cells. Data are shown with SD (n = 5–6).

Potential function of AeSCP-2L2 in lipid uptake

AeSCP-2L2 binds to both fatty acid and cholesterol, although with a higher affinity to fatty acid (19). The protein structure of AeSCP-2L2 demonstrates that fatty acid can be bound to AeSCP-2L2 at a 3:2 molar ratio. Whether this structural possibility has any biological significance regarding lipid transport is unknown. To examine the potential function of AeSCP-2L2 in vivo, we measured AeSCP-2L2-mediated lipid uptake in cultured mosquito cells and in blood-fed adult females. Overexpression of AeSCP-2L2 in Aag-2, an *A. aegypti* cell line, resulted in a significant increase ($P < 0.003$) of [^{3}H]palmitic acid uptake by 22% (**Fig. 4**) compared with a control experiment. In contrast, overexpression of AeSCP-2L2 did not cause a significant increase of cholesterol uptake (Fig. 4). These results suggest that AeSCP-2L2 is involved in fatty acid uptake in cultured cells.

Both AeSCP-2 and AeSCP-2L2 are expressed in the larvae and adults, with very similar temporal and spatial transcription profiles (18–20). To investigate the role of AeSCP-2L2 fatty acid uptake from a blood meal in adults, newly emerged adult females were injected via thoracic segments with dsRNA to knock down the expression of *AeSCP-2L2* or *AeSCP-2*. The microinjection of gene-specific dsRNAs suppressed *AeSCP-2* (18) and *AeSCP-2L2* expression (**Fig. 5A**). Three days after the dsRNA microinjection, the females were given an artificial blood meal containing [^{3}H]palmitic acid or [^{3}H]cholesterol. At the end of oogenesis (72 h after the blood meal), ovaries and the fat body were collected from each individual. Lipids were extracted from collected tissues, and the labeled palmitic acid was quantified. There was an insignificant decrease ($P > 0.38$) in overall accumulated labeled palmitic acid in *AeSCP-2L2* knockdown mosquitoes (Fig. 5B). However, knockdown of *AeSCP-2L2* corresponded to a significant ($P < 0.006$) decrease of [^{3}H]palmitic acid in the fat body, even though the uptake of [^{3}H]palmitic acid in the ovary was not affected (Fig. 5B). This decrease of labeled palmitic acid in the fat body is unlikely to be attributable to metabolic breakdown, because *AeSCP-2* knockdown did not have any effect on [^{3}H]palmitic acid uptake in either the fat body or the ovary (Fig. 5B).

Knockdown of *AeSCP-2L2* did not have any effect on [^{3}H]cholesterol uptake from the blood meal in either the fat body or the ovary (Fig. 5C), which is consistent with the fact that *AeSCP-2L2* overexpression did not have a significant ($P > 0.12$) effect on [^{3}H]cholesterol uptake in cultured cells (Fig. 4). In contrast, *AeSCP-2* knockdown significantly decreased [^{3}H]cholesterol contents in both ovaries and the fat body (Fig. 5C). This result correlates well with the observations that *AeSCP-2* affects [^{3}H]cholesterol uptake in cultured cells (10) and in larvae (18). Therefore, it is unlikely that *AeSCP-2L2* is a functional cholesterol transporter in vivo, despite its ability to bind cholesterol in vitro (19).

DISCUSSION

To date, the reported three-dimensional structures of SCP-2 family members in the Protein Data Bank include human SCP-2 (1QND), rabbit SCP-2 (1C44), mosquito SCP-2 (1PZ4), the SCP-2 domain from the human Mfe type 2 bound to Triton X-100 (1IKT), and a putative SCP-2 from the hyperthermophilic bacterium *Thermus thermo-*

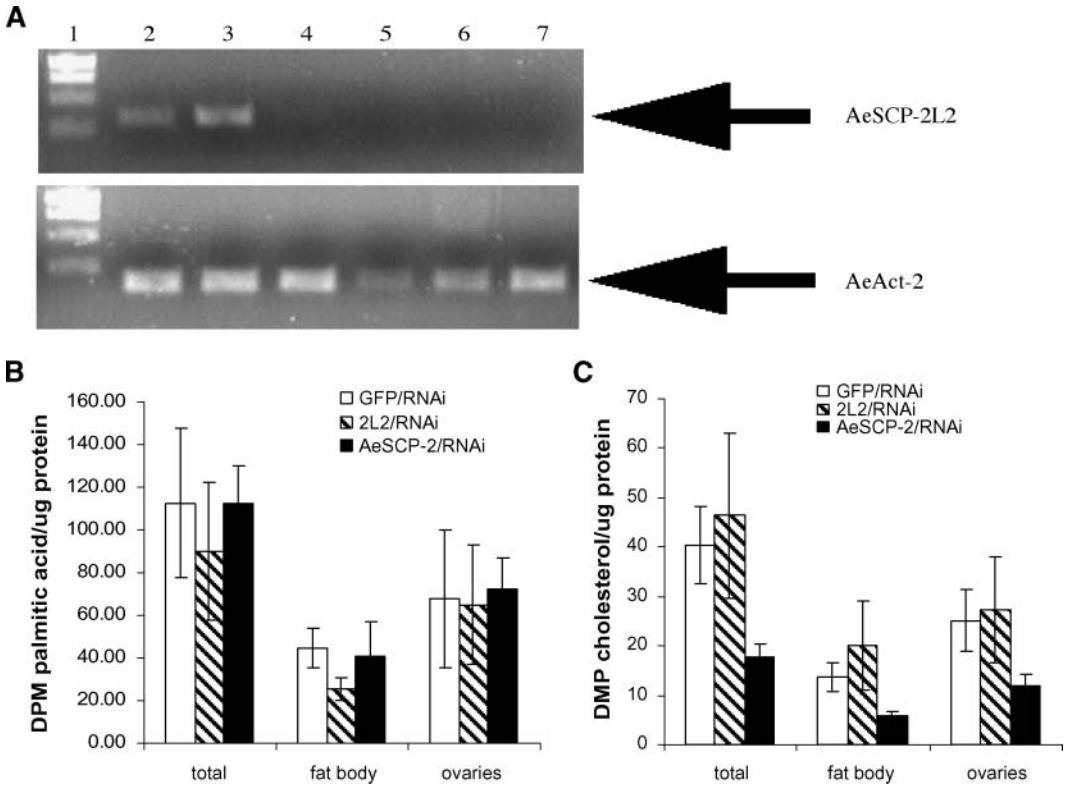

Fig. 5. Effect of *AeSCP-2* and *AeSCP-2L2* knockdown on lipid uptake in vivo. A: Expression knockdown of AeSCP-2L2 via dsRNA. Lane 1, DNA molecular weight markers; lanes 2, 3, GFP dsRNA injection controls at 24 h post blood meal (PMB); lane 4, GFP dsRNA injection control at 72 h PMB; lanes 5, 6, AeSCP-2L2 dsRNA treated at 24 h PMB; lane 7, AeSCP-2L2 dsRNA treated at 72 h PMB. The upper panel shows PCR products using AeSCP-2L2 gene-specific primers; the lower panel shows PCR products using AeAct-2 [AY289764 (30)] gene-specific primers as controls for the quality of RNAs. B: Palmitic acid uptake from a blood meal in expression knockdown females. C: Cholesterol uptake from a blood meal in expression knockdown females. Data are shown with SD (n = 5–7).

philus [2CX7 (X-ray) and 1WFR (NMR)]. The only natural ligand-bound structures are the mosquito AeSCP-2 with palmitic acid adventitiously sequestered during cell growth (1PZ4) and human Mfe type 2 bound to Triton X-100 (1IKT), which has the nonnatural detergent Triton X-100 ligated within a hydrophobic cavity. Critical differences were identified previously between the mammalian liganded SCP-2 and AeSCP-2 (21). Besides the additional short α-helix before β1 in 1IKT, the orientation of the ligand was in a horizontal position relative to the palmitate in AeSCP-2. The same can be said for AeSCP-2L2, which has a loop between α1 and β1 integral to the coordination of the fatty acid carboxylic head group. Now with the addition of AeSCP-2L2 to the SCP-2 structural gallery, it is clear that the mosquito AeSCP-2L2 possesses the ability to bind natural ligands in both the vertical and horizontal orientations. An interesting difference between the horizontal ligand binding of the human SCP-2 domain and the horizontal C16 in SCP-2L2 is that they are coordinated through hydrogen bonds on opposite sides of the protein (Fig. 3).

AeSCP-2L2 has higher affinity for free fatty acids than for cholesterol (19). The structural basis for this selectivity is unknown. It has been shown that ligand specificity is determined by a single amino acid substitution in *Euphorbia lagascae* SCP-2 and *Arabidopsis thaliana* SCP-2 (37). The *E. lagascae* SCP-2 mediates fatty acid transfer, whereas changing Leu99 to Met99 is sufficient to convert *E. lagascae* SCP-2 into a sterol-sensitive BODIPY-PC-transfer protein (37). The *A. thaliana* SCP-2 mediates the transfer of sterol. Mutating Met100 to Leu100 abolished the sterol sensitivity of *A. thaliana* SCP-2 (37). In AeSCP-2L2, the corresponding position of *E. lagascae* SCP-2 Leu99 is AeSCP-2L2 Ile89. AeSCP-2L2 Ile89 is within 4.5 Å from C10 and C13 of the horizontally bound palmitic acid in chain A and is 4.1 Å from C16 of the vertically bound palmitic acid in chain B (see supplementary Table I). It is possible that Ile89 in AeSCP-2L2 (**Fig. 6**) contributes to its higher affinity for fatty acid than for cholesterol. On the other hand, AeSCP-2 has much higher affinity for cholesterol than does AeSCP-2L2 (19, 20). AeSCP-2 Met90 corresponds to the *A. thaliana* SCP-2 Met100. It is possible that this sterol binding selectivity may be partially determined by AeSCP-2 Met90, as it is for the *A. thaliana* SCP-2 Met100. A more detailed study of the relationships between ligand specificity and the amino acid residues within the ligand binding cavity in AeSCP-2 is in progress.

With the addition of another liganded protein structure of the SCP-2 family in the yellow fever mosquito, AeSCP-2L2 demonstrates that prediction of the specificity of binding fats to this family of proteins is difficult at best. The identification of the vertical fat binding site in

Supplemental Material can be found at:
http://www.jlr.org/content/suppl/2007/12/27/M700460-JLR200.DC1.html

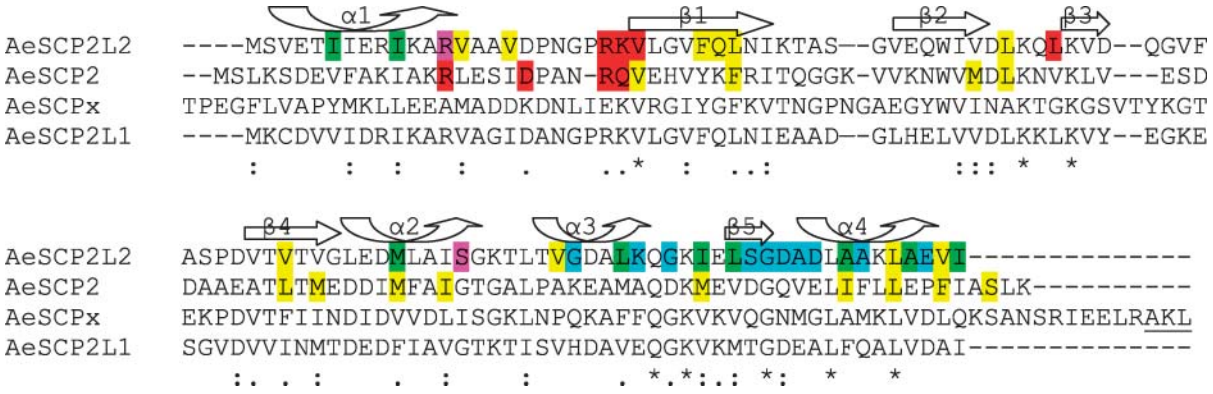

Fig. 6. Amino acid sequence alignment of members of the yellow fever mosquito SCP-2 protein family. The list shows *Aedes aegypti* SCP-2 (AAO34708), SCP-2L1 (ABF06628), SCP-2L2 (ABF38969), and SCP-x (AAQ24505). The alignment was prepared with the program CLUSTAL W version 1.8 (43). The peroxisome targeting sequence (AKL or SKL) at the C termini is underlined. The secondary structural elements correspond to the structure of yellow fever mosquito SCP-2L2, where the residues in contact with the hydrophobic acyl chain are highlighted in yellow (fatty acid in vertical position) and green (fatty acid in horizontal position); those that coordinate the carboxyl moiety are depicted in red (fatty acid in vertical position) and purple (fatty acid in horizontal position); and those forming the dimer interface are shown in blue. The residues that contact the fatty acid in AeSCP-2 are depicted with a similar color scheme.

AeSCP-2L2 using Arg23 in a water-mediated coordination of the carboxylate oxygen of the fat is different from the use of Arg15 in AeSCP-2, which shows ligation of the fat mediated by interactions through not one but two waters (21). Also, to emphasize the discrepancy between sequence predictions of ligand binding within the mosquito SCP-2 family of proteins, the equivalent position of Arg15 in AeSCP-2 is Arg13 in AeSCP-2L2, which is critical, along with Ser74, for coordination of the horizontal fat. The common feature that identifies a fatty acid binding site appears to include variations on a theme of electrostatic interactions with polar and basic side chains to coordinate the carboxylate head group of the fat. It should be noted that arginine side chain interactions with fats have been observed in other protein structures with very different folds (35, 38, 39, 40, 41).

The dimer interface is organized via the C-terminal region (α3, β5, and α4). However, only 3 of the 13 residues (Fig. 6, blue residues) involved in the dimer interface interaction are conserved (23% similarity), compared with 11 of the 27 residues conserved in this region of the SCP-2 domain (41% similarity) among all members of SCP-2 and SCP-2-like proteins (Fig. 6). Therefore, it is possible that the dimerization is a phenomenon unique to AeSCP-2L2. Evolutionary constraints on the three-dimensional architecture of the sterol carriers/nonspecific lipid carriers may be responsible for the conservation of both lipid orientations found in SCP-2L2. The biological necessity to transfer lipids in insects and in humans from different orientations may apply to very specific needs at the cellular level.

It is evident that nonperoxisomal SCP-2 genes are expanded evolutionarily in mosquitoes. In the yellow fever mosquito, there are at least four genes that produce low molecular weight proteins containing only the SCP-2 domain (19, 20, 42). AeSCP-x is a more distantly related protein to AeSCP-2 and AeSCP-2-like proteins based on phylogenic analysis (19). In fact, the posttranslational product of AeSCP-x is the only low molecular weight member of the SCP-2 protein family with the peroxisome-targeting sequences (Fig. 6), and it is mostly localized to the peroxisome (10). Thus, it is highly likely that AeSCP-x's function is restricted to lipid metabolism in the peroxisome, whereas other members of the nonperoxisomal SCP-2 and SCP-2-like proteins may function as intracellular lipid carriers in the cytosol. To determine whether those proteins have overlapping functions, a comparative approach is needed at the genetic, molecular, and physiological levels.

Results from previous studies suggest that AeSCP-2 is involved in cholesterol uptake in both cultured cells and larvae (10, 18). The transcription profiles indicate that AeSCP-2 and AeSCP-2L2 have very similar temporal and spatial expression patterns (18–20). In this study, a direct comparison was made to examine lipid uptake via AeSCP-2 and AeSCP-2L2 in adult females. Those two proteins clearly play different roles in cholesterol and free fatty acid uptake in vivo (Fig. 5B, C). These results are consistent with the observation that AeSCP-2 has high affinity for cholesterol (20), whereas AeSCP-2L2 has greater affinity for free fatty acid than for cholesterol (19). Therefore, despite the three-dimensional structural similarities between AeSCP-2 and AeSCP-2L2, the differences in their affinities for ligands may contribute to the dissimilarity in their biological functions.

The authors thank Mr. Jeffrey M. Lorch for technical assistance. This work was supported by the University of Wisconsin-Madison College of Agriculture and Life Sciences' U. S. Department of Agriculture- The Cooperative State Research, Education, and Extension Service (CSREES) Hatch Project WIS04963, by Grant W9113M-05-1-0006 from the Deployed War Fighter Protection Research Program administered by the U. S. Armed Forces Pest Management Board, and by National Institutes of Health Research Grant 5R01 AI-067422 to Q.L.

REFERENCES

1. Noland, B. J., R. E. Arebalo, E. Hansbury, and T. J. Scallen. 1980. Purification and properties of sterol carrier protein2. *J. Biol. Chem.* **255:** 4282–4289.
2. Puglielli, L., A. Rigotti, A. V. Greco, M. J. Santos, and F. Nervi. 1995. Sterol carrier protein-2 is involved in cholesterol transfer from the endoplasmic reticulum to the plasma membrane in human fibroblasts. *J. Biol. Chem.* **270:** 18723–18726.
3. Frolov, A., J. K. Woodford, E. J. Murphy, J. T. Billheimer, and F. Schroeder. 1996a. Spontaneous and protein-mediated sterol transfer between intracellular membranes. *J. Biol. Chem.* **271:** 16075–16083.
4. Gallegos, A. M., J. K. Schoer, O. Starodub, A. B. Kier, J. T. Billheimer, and F. Schroeder. 2000. A potential role for sterol carrier protein-2 in cholesterol transfer to mitochondria. *Chem. Phys. Lipids.* **105:** 9–29.
5. Moncecchi, D., E. J. Murphy, D. R. Prows, and F. Schroeder. 1996. Sterol carrier protein-2 expression in mouse L-cell fibroblasts alters cholesterol uptake. *Biochim. Biophys. Acta.* **1302:** 110–116.
6. Atshaves, B. P., S. M. Storey, A. L. McIntosh, A. D. Petrescu, O. I. Lyuksyutova, A. S. Greenberg, and F. Schroeder. 2001. Sterol carrier protein-2 expression modulates protein and lipid composition of lipid droplets. *J. Biol. Chem.* **276:** 25324–25335.
7. Gallegos, A. M., B. P. Atshaves, S. M. Storey, A. L. McIntosh, A. D. Petrescu, and F. Schroeder. 2001. Sterol carrier protein-2 expression alters plasma membrane lipid distribution and cholesterol dynamics. *Biochemistry.* **40:** 6493–6506.
8. Murphy, E. J. 2002. Sterol carrier protein-2: not just for cholesterol any more. *Mol. Cell. Biochem.* **239:** 87–93.
9. Atshaves, B. P., S. M. Storey, and F. Schroeder. 2003. Sterol carrier protein-2/sterol carrier protein-x expression differentially alters fatty acid metabolism in L cell fibroblasts. *J. Lipid Res.* **44:** 1751–1762.
10. Lan, Q., and R. J. Massey. 2004. Subcellular localization of mosquito sterol carrier protein-2 and sterol carrier protein-x. *J. Lipid Res.* **45:** 1468–1474.
11. Frolov, A., T. H. Cho, J. T. Billheimer, and F. Schroeder. 1996b. Sterol carrier protein-2, a new fatty acyl coenzyme A-binding protein. *J. Biol. Chem.* **271:** 31878–31884.
12. Stolowich, N., A. Frolov, A. D. Petrescu, A. I. Scott, J. T. Billheimer, and F. Schroeder. 1999. Holo-sterol carrier protein-2. (13)C NMR investigation of cholesterol and fatty acid binding sites. *J. Biol. Chem.* **274:** 35425–35433.
13. Schroeder, F., A. Frolov, O. Starodub, B. B. Atshaves, W. Russell, A. Petrescu, H. Huang, A. M. Gallegos, A. McIntosh, D. Tahotna, et al. 2000. Pro-sterol carrier protein-2: role of the N-terminal presequence in structure, function, and peroxisomal targeting. *J. Biol. Chem.* **275:** 25547–25555.
14. Kannenberg, F., P. Ellinghaus, G. Assmann, and U. Seedorf. 1999. Aberrant oxidation of the cholesterol side chain in bile acid synthesis of sterol carrier protein-2/sterol carrier protein-x knockout mice. *J. Biol. Chem.* **274:** 35455–35460.
15. Fuchs, M., A. Hafer, C. Munch, F. Kannenberg, S. Teichmann, J. Scheibner, E. F. Stange, and U. Seedorf. 2001. Disruption of the sterol carrier protein 2 gene in mice impairs biliary lipid and hepatic cholesterol metabolism. *J. Biol. Chem.* **276:** 48058–48065.
16. Ohba, T., J. A. Holt, J. T. Billheimer, and J. F. Strauss, 3rd. 1995. Human sterol carrier protein x/sterol carrier protein 2 gene has two promoters. *Biochemistry.* **34:** 10660–10668.
17. Gallegos, A. M., B. P. Atshaves, S. M. Storey, O. Starodub, A. D. Petrescu, H. Huang, A. McIntosh, G. Martin, H. Chao, A. B. Kier, et al. 2001. Gene structure, intracellular localization, and functional roles of sterol carrier protein-2. *Prog. Lipid Res.* **40:** 498–563.
18. Blitzer, E. J., I. Vyazunova, and Q. Lan. 2005. Functional analysis of AeSCP-2 using gene expression knockdown in the yellow fever mosquito, *Aedes aegypti*. *Insect Mol. Biol.* **14:** 301–307.
19. Vyazunova, I., V. Wessley, M. Kim, and Q. Lan. 2007. Identification of two sterol carrier protein-2 like genes in the yellow fever mosquito, *Aedes aegypti*. *Insect Mol. Biol.* **16:** 305–314.
20. Krebs, K. C., and Q. Lan. 2003. Isolation and expression of a sterol carrier protein-2 gene from the yellow fever mosquito, *Aedes aegypti*. *Insect Mol. Biol.* **12:** 51–60.
21. Dyer, D. H., S. Lovell, J. B. Thoden, H. M. Holden, I. Rayment, and Q. Lan. 2003. The structural determination of an insect sterol carrier protein-2 with a ligand bound C16 fatty acid at 1.35A resolution. *J. Biol. Chem.* **278:** 39085–39091.
22. de La Fortelle, E., and G. Bricogne. 1997. Maximum-likelihood heavy-atom parameter refinement for multiple isomorphous replacement and multiwavelength anomalous diffraction methods. *Methods Enzymol.* **276:** 472–494.
23. Perrakis, A., R. Morris, and V. S. Lamzin. 1999. Automated protein model building combined with iterative structure refinement. *Nat. Struct. Biol.* **6:** 458–463.
24. Murshudov, G. N., A. A. Vagin, and E. J. Dodson. 1997. Refinement of macromolecular structures by the maximum-likelihood method. *Acta Crystallogr. D Biol. Crystallogr.* **53:** 240–255.
25. McRee, D. E. 1999. XtalView/Xfit—a versatile program for manipulating atomic coordinates and electron density. *J. Struct. Biol.* **125:** 156–165.
26. Laskowski, R. A., M. W. MacArthur, D. S. Moss, and J. M. Thornton. 1993. PROCHECK: a program to check the stereochemical quality of protein structures. *J. Appl. Cryst.* **26:** 283–291.
27. Lan, Q., A. Gerenday, and A. M. Fallon. 1993. Cultured *Aedes albopictus* mosquito cells synthesize hormone-inducible proteins. *In Vitro Cell. Dev. Biol.* **29A:** 813–818.
28. Lan, Q., K. Hiruma, X. Hu, M. Jindra, and L. M. Riddiford. 1999. Activation of a delayed-early gene encoding MHR3 by the ecdysone receptor heterodimer EcR-B1-USP-1 but not by EcR-B1-USP-2. *Mol. Cell. Biol.* **19:** 4897–4906.
29. Beerntsen, B. T., and B. M. Christensen. 1990. *Dirofilaria immitis*: effect on hemolymph polypeptide synthesis in *Aedes aegypti* during melanotic encapsulation reactions against microfilariae. *Exp. Parasitol.* **71:** 406–414.
30. Vyazunova, I., and Q. Lan. 2004. Stage-specific expression of two actin genes in the yellow fever mosquito, *Aedes aegypti*. *Insect Mol. Biol.* **13:** 241–249.
31. Kogan, P. H. 1990. Substitute blood meal for investigating and maintaining *Aedes aegypti* (Diptera: Culicidae). *J. Med. Entomol.* **27:** 709–712.
32. Murzin, A. G., S. E. Brenner, T. Hubbard, and C. Chothia. 1995. SCOP: a structural classification of proteins database for the investigation of sequences and structures. *J. Mol. Biol.* **247:** 536–540.
33. Jones, S., and J. M. Thornton. 1996. Principles of protein-protein interactions derived from structural studies. *Proc. Natl. Acad. Sci. USA.* **93:** 13–20.
34. Connolly, M. L. 1983. Solvent-accessible surfaces of proteins and nucleic acids. *Science.* **221:** 709–713.
35. Choinowski, T., H. Hauser, and K. Piontek. 2000. Structure of sterol carrier protein 2 at 1.8 Å resolution reveals a hydrophobic tunnel suitable for lipid binding. *Biochemistry.* **39:** 1897–1902.
36. Haapalainen, A. M., D. M. van Aalten, G. Merilainen, J. E. Jalonen, P. Pirila, R. K. Wierenga, J. K. Hiltunen, and T. Glumoff. 2001. Crystal structure of the liganded SCP-2-like domain of human peroxisomal multifunctional enzyme type 2 at 1.75 Å resolution. *J. Mol. Biol.* **313:** 1127–1138.
37. Juers, D. H., and B. W. Matthews. 2004. Cryo-cooling in molecular crystallography: advantages, disadvantages and optimization. *Q. Rev. Biophys.* **37:** 105–119.
38. Thompson, J. R., and L. J. Banaszak. 2002. Lipid-protein interactions in lipovitellin. *Biochemistry.* **41:** 9398–9409.
39. Viitanen, L., M. Nylund, D. M. Eklund, C. Alm, A. K. Eriksson, J. Tuuf, T. A. Salminen, P. Mattjus, and J. Edqvist. 2006. Characterization of SCP-2 from *Euphorbia lagascae* reveals that a single Leu/Met exchange enhances sterol transfer activity. *FEBS J.* **273:** 5641–5655.
40. Reese, A. J., and L. J. Banaszak. 2004. Specificity determinants for lipids bound to β-barrel proteins. *J. Lipid Res.* **45:** 232–243.
41. Bhattacharya, A. A., T. Grune, and S. Curry. 2000. Crystallographic analysis reveals common modes of binding of medium and long chain fatty acids to human serum albumin. *J. Mol. Biol.* **303:** 721–732.
42. Lan, Q., and V. Wessely. 2004. Expression of a sterol carrier protein-x gene in the yellow fever mosquito, *Aedes aegypti*. *Insect Mol. Biol.* **13:** 519–529.
43. Thompson, J. D., D. G. Higgins, and T. J. Gibson. 1994. CLUSTAL W: improving the sensitivity of progressive multiple sequence alignment through sequence weighting, position-specific gap penalties and weight matrix choice. *Nucleic Acids Res.* **22:** 4673–4680.